IAC-14-C1.9.11

TRAJECTORY DESIGN FOR BOUNDED MOTION NEAR UNCERTAIN BINARY SYSTEMS COMPRISED OF SMALL IRREGULAR BODIES EXPLOITING SLIDING CONTROL MODES

Loic Chappaz*
Purdue University, United States of America
lchappaz@purdue.edu

Kathleen C. Howell†
Purdue University, United States of America
howell@purdue.edu

To investigate the behavior of a spacecraft near a pair of irregular bodies, consider a three body configuration (one massless). Two massive bodies, P_1 and P_2, form the primary system; each primary is initially modeled as an ellipsoid. Concepts and tools similar to those applied in the Circular Restricted Three-Body Problem (CRTBP) are exploited to construct bounded trajectories for a third body in such a synchronous system. Then, to accommodate model uncertainties and other non-gravitational perturbations, a design strategy to maintain a spacecraft near a reference path is proposed.

I. INTRODUCTION

While most of the more massive bodies in the solar system are reasonably spherical, there are many smaller objects with very irregular shapes. Such small bodies may orbit the Sun, a planet, or even an asteroid or other small body. These irregular objects are the focus of increasing scientific interest and their study, through various types of observations, offers insight into the early development of the solar system, as well as the formation and origin of more massive bodies. However, ground-based observations possess limited capabilities and closer observations, available during in situ missions, supply higher volume and higher quality data for analysis. Yet, to successfully design trajectories to reach such small, arbitrarily-shaped bodies and to explore the nearby regions, a more thorough understanding of the dynamical environment in the vicinity of such systems is required.

In recent years, several spacecraft have been delivered to the vicinity of small irregular bodies and more complex missions are under development. In 2001, after a series of orbital revolutions to bring the NEAR spacecraft closer to the asteroid 433 Eros and to gather more scientific observations, the vehicle landed on the asteroid surface.[1] Launched in 2007, the current Dawn project is another mission to multiple irregular bodies, with a spacecraft that orbited Vesta for over a year and is now enroute to the dwarf planet Ceres.[2] The Russian Phobos-Grunt spacecraft, launched in November 2011, originally planned to land a probe on Phobos and return a soil sample to Earth; unfortunately, the spacecraft never left Earth orbit.[3] Currently, ESA's Rosetta spacecraft is orbiting comet 67P/ChuryumovGerasimenko and will deliver a lander to the comet's surface for further exploration of this very irregular body.[4] In 2016, the NASA mission OSIRIS-REX is scheduled to deliver a spacecraft to the asteroid 1999 RQ36 to collect soil samples and to investigate this potentially hazardous object.[5] Based on such initial steps, the number of proposals involving such spacecraft destinations is generally increasing. In addition, current estimates indicate that approximately sixteen percent of the known near-Earth asteroid population may be binaries[6] and a few new mission concepts are emerging to visit binary systems comprised of irregular bodies. Thus, further exploration of the dynamical behavior in such an environment is warranted. In support of such future endeavors, previous analyses have investigated the dynamical environment in the vicinity of a pair of irregularly-shaped bodies with a ellipsoid-sphere model,[7,8] and some investigations have been completed with alternative approaches that are based on modeling of the primary bodies as geometric polyhedra.[9,10] Such models have also been previously applied to scenarios that involve a single asteroid.[11]

The focus of the analysis in this work is the behavior of a third body in the vicinity of a system comprised of two irregular bodies that might represent a binary.

*PhD Student, School of Aeronautics and Astronautics
†Hsu Lo Distinguished Professor of Aeronautics and Astronautics, College of Engineering

Previous work from the authors[8,12] focused on the exploration of bounded trajectories in the vicinity of a simplified system. However, these types of dynamical models are idealized representations of the actual dynamical regime and do not incorporate uncertainties in the physical properties of the bodies and other non-gravitational perturbing effects. In this analysis, a trajectory design strategy to maintain a spacecraft near reference third-body trajectories that exhibit some desired characteristics is constructed incorporating multiple sliding surfaces guidance.[13,14] Such a control law can be demonstrated to be globally stable and robust. In practical applications, the exact physical properties of the massive bodies in the system are not known. It is reasonable to assume sufficient knowledge to construct an 'estimated' model that approximates the properties of the 'true' system. For the true system, each primary is modeled as a polyhedron and the 'estimated' system employs a sphere-ellipsoid or an ellipsoid-ellipsoid model. Then, to maintain the spacecraft in orbit near a desired reference path, a 'coast and thrust' scheme is proposed.

II. DYNAMICAL MODEL DEVELOPMENT

Within the context of trajectory exploration near systems comprised of small irregular bodies, a first step in the analysis is the development of a dynamical model that describes the motion of the primary system. Then, to incorporate the motion of a third body, additional dynamical models that describe the third-body behavior for different levels of complexity in the primary system model are constructed.

II.I Idealized Dynamical Model

Consider an initial idealized dynamical model such that the primary system is comprised of two rotating ellipsoids, i.e., both P_1 and P_2 are modeled as tri-axial constant density ellipsoids with semi-major axes α_i, β_i, and γ_i for the bodies P_i, $i = 1, 2$. The motion of the isolated primary system is first addressed before deriving the equations that govern the behavior of a third massless body near such a system.

Motion of the primary system

One strategy to derive the equations of motion that describe the time evolution of such a system is to assume that the mutual orbit of the two ellipsoids is coplanar and equatorial. Then, the problem can be fully described with four degrees of freedom, q_i, in terms of one distance and three angles.[15] First, an inertially fixed frame $(\hat{e_1}, \hat{e_2}, \hat{e_3})$ is defined such that the plane spanned by $(\hat{e_1}, \hat{e_2})$ is parallel to the orbital plane of the primary system. Then, a second frame is defined consistent with the rotating frame in the Circular Restricted Three-Body Problem (CRTBP), that is, the first base vector $\hat{s_1}$ is directed from P_1 to P_2 between the centers of mass, $\hat{s_3}$ is parallel to the orbital angular velocity of the primary system, and $\hat{s_2}$ completes the right-handed unit vector basis. Thus, the inertial and orbital frames are related via a rotation about the inertial direction $\hat{e_3} = \hat{s_3}$ through the angle θ. Also, both ellipsoids are assumed to be rotating about the third inertial direction, $\hat{e_3}$, such that the orientation between the body fixed-frame $(\hat{x_i}, \hat{y_i}, \hat{z_i})$ moving with the primary i and the orbital frame is fully described by the angle ϕ_i. Consequently, $\hat{e_3} = \hat{z_1} = \hat{z_2}$. Finally, the distance r denotes the separation between the two primary bodies, as illustrated in Figure 1. Then, the Lagrangian equations of the motion for the primary system, of the form $d\left(\partial L/\partial \dot{q_i}\right)/dt = \partial L/\partial q_i$, are derived as follows,

$$\ddot{r} = \dot{\theta} r - \frac{1}{m} U_r \quad [1]$$

$$\ddot{\phi_1} = -\left(1 + \frac{mr^2}{I_{1_z}}\right) \frac{1}{mr^2} U_{\phi_1} - \frac{1}{mr^2} U_{\phi_2} + 2\frac{\dot{r}\dot{\theta}}{r} \quad [2]$$

$$\ddot{\phi_2} = -\left(1 + \frac{mr^2}{I_{2_z}}\right) \frac{1}{mr^2} U_{\phi_2} - \frac{1}{mr^2} U_{\phi_1} + 2\frac{\dot{r}\dot{\theta}}{r} \quad [3]$$

$$\ddot{\theta} = \frac{1}{mr^2}\left(U_{\phi_1} + U_{\phi_2}\right) - 2\frac{\dot{r}\dot{\theta}}{r} \quad [4]$$

where m denotes the reduced mass of the primary system defined as $m = m_1 m_2/(m_1 + m_2)$. Then, $U_r = \partial U/\partial r$, $U_{\phi_1} = \partial U/\partial \phi_1$, and $U_{\phi_2} = \partial U/\partial \phi_2$ and U is the potential energy of the system defined as,

$$U(r, \phi_1, \phi_2) = -\frac{Gm_1 m_2}{r}\left\{1 + \frac{1}{2r^2}\left[Tr(\bar{\bar{I}}_1) + Tr(\bar{\bar{I}}_2) - \frac{3}{2}\left(I_{1_x} + I_{1_y} - \cos 2\phi_1 \left(I_{1_y} - I_{1_x}\right) + I_{2_x} + I_{2_y} - \cos 2\phi_2 \left(I_{2_y} - I_{2_x}\right)\right)\right]\right\} \quad [5]$$

where G is the universal gravitational constant and $\bar{\bar{I}}_1$ and $\bar{\bar{I}}_2$ represent the inertia dyadics associated with P_1 and P_2, respectively, such that $\bar{\bar{I}}_i = diag\left[I_{i_x}, I_{i_y}, I_{i_z}\right], i = 1, 2$.

Three-body dynamical model (EETBP)

The motion of a massless third body is modeled assuming that the primary system is comprised of the two massive ellipsoids, P_1 and P_2, as illustrated in Figure 1. Note in the figure that the third particle is located relative to the first primary, P_1, center of mass, as viewed in the inertially-fixed frame, by the position vector $\bar{\rho} = x\hat{e}_1 + y\hat{e}_2 + z\hat{e}_3$. Similar to the full two-body problem, the equations of the motion that describe the behavior of a massless particle near a primary system are derived from Newton's second law.

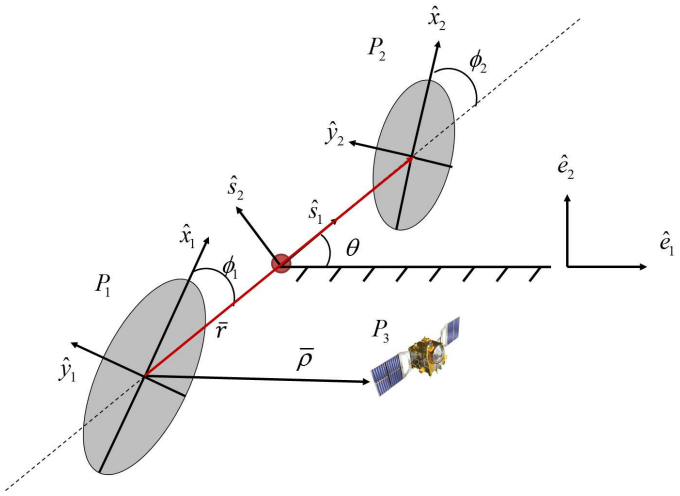

Fig. 1: Ellipsoid-ellipsoid full two-body problem and three-body problem geometry

Expressed with respect to the inertial frame, the 2nd-order vector EOM is,

$$\ddot{\bar{\rho}} = \frac{\partial U_{EE}}{\partial \bar{\rho}} \qquad [6]$$

where the symbol U_{EE} then denotes the gravitational potential defined as $U_{EE} = (1-\mu)U_{e_1} + \mu U_{e_2}$; U_{e_1} and U_{e_2} represent the potentials that are associated with P_1 and P_2, respectively. Similar to the CRTBP, where no complete analytical solution to the EOMs exists, this set of differential equations is also numerically integrated along with the full-two body problem EOMs to simulate the motion of a massless third particle.

Synchronous systems

From the general formulation, two equilibrium primary configurations are identified: the long-axis equilibrium and the short-axis equilibrium configurations. Initially, consider the long-axis configuration, that is, a primary orientation such that the two ellipsoids' largest semi-major axis directions, α_1 and α_2, are each aligned with the ellipsoid-ellipsoid direction $\hat{s}_1$. For this configuration to be maintained, both rotating frames coincide and the primaries P_1 and P_2 appear to be fixed in the rotating frame. This configuration is labeled 'synchronous'. Also true in synchronous systems, the angular velocity $\dot{\theta}$ is constant in magnitude.

II.II High-Fidelity Dynamical Model

An alternate higher-fidelity approach to the ellipsoidal shape model for the representation of the primaries in a given system is a model that constructs each body as a constant density polyhedron. There is no restriction on the geometric complexity in the polyhedron model; as a consequence, the relative orbital motion and the attitude orientation of the two bodies are coupled.

Motion of the primary system

The differential equations for the coupled relative motion of a primary system, such that each massive body is an arbitrarily-shaped but constant density polyhedron, can be numerically integrated. One approach exploits a semi-implicit Lie Group Variational Integrator (LGVI) and the discretized equations of the motion for the full two-body problem as expressed in a frame that is fixed with and centered at the primary P_1.[9,16] The scalar EOMs are coupled and include both the relative orbital motion as well as the attitude of the two bodies as time evolves. As part of the integration process, the mutual forces and moments, that is, the resultant force and moment that each body exerts on the other, must be evaluated. There is no known exact method to compute these quantities for a pair of arbitrary polyhedra; rather, the algorithm relies on an infinite series expansion of the gravitational potential function. Then, the force and moment terms are computed as the derivatives of the approximated potential function with respect to the relative position vector and the relative attitude matrix, respectively.[17,18] The numerical integration is computationally expensive and a trade-off between the resolution of the discretization for each shape model and the number of terms to include in the series expansion for the gravitational potential approximation is necessary to achieve reasonable computation times. For this analysis, a C++ program that leverages a Message Passing Interface (MPI) is employed for the integration of the relative motion for a given binary system. Simulations are performed on Purdue University's Coates cluster using up to 2800 cores (350 nodes).

Three-body dynamical model (PPTBP)

The motion of a massless third body is modeled assuming that the primary system is comprised of the two constant density polyhedra, P_1 and P_2, where the

relative motion of the primary system is pre-computed. Note that the third particle is located relative to the primary P_1 center of mass, as viewed in the inertially-fixed P_1-centered frame. (See Figure 1.) However, the problem can be similarly formulated for either primary as the central body. The equations of motion that describe the behavior of a massless particle near such a primary system are similar to the ellipsoid-ellipsoid problem, as expressed with respect to the inertial frame in Eq. [6] where the symbol U_{EE} is replaced with U_{PP}. The symbol U_{PP} now denotes the gravitational potential defined as $U_{PP} = (1-\mu)U_{p_1} + \mu U_{p_2}$ where U_{p_1} and U_{p_2} represent the potentials that are associated with the polyhedra P_1 and P_2, respectively. In contrast to the motion of the primary system, where the mutual gravitational potential is expressed in terms of an infinite series, the gravitational potential that is exerted on the massless third body by each polyhedron can be computed independently. For each gravitational potential, and consequently the gravitational force, exerted by a single constant density polyhedron onto a massless particle, there exists an exact closed-form solution.[19] Thus, the gravitational potential is exact for a given shape and density. The resolution of the calculated field depends directly upon the level of discretization selected for a particular shape. However, the polyhedron is still an approximation for the actual shape of the body and the accuracy of the gravity field is consistent with its shape determination. In addition, the Solar Radiation Pressure (SRP) that is exerted on a spacecraft is a significant perturbing acceleration, especially in a scenario that involves small bodies, such as asteroids. In this analysis, a simple model that assumes the spacecraft is spherical and possesses a constant reflectivity is employed to include this perturbation effect into the model.

III. MULTIPLE SLIDING SURFACES GUIDANCE (MSSG)

A robust guidance law to control the motion of a spacecraft in the vicinity of a pair of irregular bodies is introduced. The multiple sliding surfaces guidance[13,14] development relies on higher order sliding control theory.[20,21] The objective is to develop an acceleration law, one that is robust against unmodeled perturbations, and sufficiently flexible to accommodate the design objectives.

III.I MSSG guidance law development

To explore and direct the behavior of a spacecraft near a binary system comprised of irregular bodies, the objective is an acceleration guidance law that is robust against unmodeled perturbing effects. Since the gravity field is an approximation and additional unmodeled forces may exist, such a strategy offers an effective assessment tool. Initially consider the derivation of the MSSG guidance law without perturbing accelerations. First, rewrite the vector EOMs, as expressed in terms of the inertial frame, in a first-order form,

$$\dot{\bar{\rho}} = \bar{v} \quad [7]$$

$$\dot{\bar{v}} = \frac{\partial U}{\partial \bar{\rho}} + \bar{a}_c \quad [8]$$

where $\bar{a}_c$ is the acceleration command. It is clear that the control $\bar{a}_c$ appears in the second time derivative of the output, that is, $\ddot{\bar{\rho}}$ or $\dot{\bar{v}}$. Thus, the motion of the guided spacecraft exists on a 2-sliding mode. For a 2-sliding mode control scheme,[20,21] the goal is the selection of a sliding surface vector $\bar{s}$ such that $\bar{s} = \dot{\bar{s}} = \bar{0}$ when the control objective is achieved. Also, the dynamics of the sliding system must possess relative degree 2, that is, the acceleration command appears in the second time derivative of the sliding surface vector. Define a first sliding vector surface as,

$$\bar{s}_1 = \bar{\rho} - \bar{\rho}_D \quad [9]$$

where $\bar{\rho}_D$ is the desired nondimensional position vector of the spacecraft. Differentiating $\bar{s}_1$ with respect to time yields,

$$\dot{\bar{s}}_1 = \dot{\bar{\rho}} - \dot{\bar{\rho}}_D = \bar{v} - \bar{v}_D \quad [10]$$

where $\bar{v}_D$ is the desired nondimensional velocity vector of the spacecraft. Note that the sliding surface is, in fact, of relative degree 2. The second time derivative of $\bar{s}_1$ is evaluated as,

$$\ddot{\bar{s}}_1 = \dot{\bar{v}} - \dot{\bar{v}}_D = \frac{\partial U}{\partial \bar{\rho}} + \bar{a}_c - \dot{\bar{v}}_D \quad [11]$$

The guidance problem is formulated as follows: determine the acceleration command, $\bar{a}_c$, such that the sliding vector surface $\bar{s}_1$, and its time derivative, both converge to zero in a finite time, i.e., $t \to t_f, \bar{s}_1, \dot{\bar{s}}_1 \to 0$. The objective is achieved by selecting $\dot{\bar{s}}_1$ as a virtual control coupled with a backstepping method. First, $\dot{\bar{s}}_1$ is selected such that the first sliding surface reaches zero in a finite time. One choice for the virtual control such that $\bar{s}_1 \to 0$ as $t \to t_f$ is,

$$\dot{\bar{s}}_1 = -\frac{\Lambda}{t_f - t}\bar{s}_1 \quad [12]$$

where $\Lambda = diag\,[\Lambda_1\ \Lambda_2\ \Lambda_3]$ is a diagonal matrix and Λ_i are guidance gains such that $\Lambda_i > 0$. To prove that the virtual control $\dot{\bar{s}}_1$ is globally stable and, thus, effectively drives the first sliding surface to zero in a finite time, consider the candidate Lyapunov function,

$$V_1 = \frac{1}{2}\bar{s}_1^T \bar{s}_1 \quad [13]$$

Clearly, $V_1(\bar{s}_1 = \bar{0}) = 0$ and $\forall \bar{s}_1 \in \mathbb{R}^3 - \{\bar{0}\}, V_1(\bar{s}_1) > 0$, therefore V_1 is positive definite. Then,

$$\dot{V}_1 = \bar{s}_1^T \dot{\bar{s}}_1 = -\frac{1}{t_f - t} \bar{s}_1^T \Lambda \bar{s}_1 \quad [14]$$

where Λ, as recalled, is defined such that $\Lambda_i > 0$, i.e., Λ is positive definite. Then, $-\dot{V}_1$ is expressed as a quadratic form of the virtual state $\bar{s}_1$ with Λ positive definite, therefore, $\dot{V}_1$ is negative definite. Finally, with V_1 and $-\dot{V}_1$ positive definite, the Lyapunov theorem concludes that the virtual control $\dot{\bar{s}}_1$ is globally stable. A solution for the virtual state, $\bar{s}_1$, can be explicitly derived and allows further constraints on the gain matrix Λ. Applying separation of variables on Eq. [12],

$$\frac{ds_{1i}}{s_{1i}} = \frac{\Lambda_i dt}{t_f - t} \quad [15]$$

where $i = 1, 2, 3$, i.e., $\bar{s}_1 = [s_1\ s_2\ s_3]^T$. Direct integration of Eq. [15] produces,

$$\log(s_{1i}) = \Lambda_i \log(t_f - t) + C_i \quad [16]$$

where s_{1i} are the components of $\bar{s}_1$ and the vector integration constant $\bar{C}$ is explicitly defined by imposing the initial condition $\bar{s}_1(0) = \bar{s}_{10}$. Also, after evaluation of the exponential of both sides in Eq. [16], the solution results in the expression,

$$s_{1i}(t) = s_{1i_0} (t_f - t)^{\Lambda_i} \quad [17]$$

The time derivative of the sliding surface is then directly derived as,

$$\dot{s}_{1i}(t) = \Lambda_i s_{1i_0} (t_f - t)^{\Lambda_i - 1} \quad [18]$$

Provided that $\Lambda_i > 0$, Eq. [17] guarantees that the sliding surface vector converges to zero in a finite time. However, if $\Lambda_i < 1$, the time derivative of the sliding surface in Eq. [18] diverges as $t \to t_f$. Therefore, the matrix gains are selected such that $\Lambda_i > 1$ to guarantee that both the sliding surface vector and its time derivative reach zero as $t \to t_f$. Recall that the goal is an acceleration command $\bar{a}_c$ that achieves the control objective. Thus, the virtual control $\dot{\bar{s}}_1$ must be explicitly related to the acceleration command to successfully achieve the objective $\bar{s}_1, \dot{\bar{s}}_1 \to \bar{0}$. Also note that, initially, the spacecraft position and velocity vectors may not, in general, satisfy Eq. [12]. The next step in deriving the guidance law is the definition of a second sliding surface that forces the desired acceleration command to drive the virtual control from its initial value to a trajectory that follows the dynamics in the first-order nonlinear equation defined in Eq. [12]. In addition, under the acceleration command, the system must be maintained on the second surface until $\bar{s}_1, \dot{\bar{s}}_1 \to \bar{0}$ is attained. The second sliding surface vector is selected as,

$$\bar{s}_2 = \dot{\bar{s}}_1 + \frac{\Lambda}{t_f - t} \bar{s}_1 = \bar{0} \quad [19]$$

where it is easily verified that the second sliding surface is now of relative degree 1 with respect to the acceleration command, that is, $\bar{a}_c$ appears explicitly in the first time derivative of the second surface,

$$\dot{\bar{s}}_2 = \ddot{\bar{s}}_1 + \frac{\Lambda}{t_f - t} \dot{\bar{s}}_1 + \frac{\Lambda}{(t_f - t)^2} \bar{s}_1 \quad [20]$$

The expression for $\ddot{\bar{s}}_1$ derived in Eq. [11] is substituted in Eq. [20] to produce,

$$\dot{\bar{s}}_2 = \frac{\partial U}{\partial \bar{\rho}} + \bar{a}_c - \dot{\bar{v}}_D + \Lambda \frac{(t_f - t)\, \dot{\bar{s}}_1 + \bar{s}_1}{(t_f - t)^2} \quad [21]$$

To select an adequate acceleration command that guarantees global stability of the closed-loop system, the Lyapunov stability theory is again exploited. Consider the second Lyapunov candidate function,

$$V_2 = \frac{1}{2} \bar{s}_2^T \bar{s}_2 \quad [22]$$

Similar to V_1, V_2 is positive definite and its time derivative is explicitly computed as,

$$\dot{V}_2 = \bar{s}_2^T \dot{\bar{s}}_2 = \bar{s}_2^T \left[\frac{\partial U}{\partial \bar{\rho}} + \bar{a}_c - \dot{\bar{v}}_D + \Lambda \frac{(t_f - t)\, \dot{\bar{s}}_1 + \bar{s}_1}{(t_f - t)^2} \right] \quad [23]$$

Finally, for $\dot{V}_2$ to be negative definite, one possible choice for the command acceleration is,

$$\bar{a}_c(t) = -\left\{ \frac{\partial U}{\partial \bar{\rho}} - \dot{\bar{v}}_D + \Lambda \frac{(t_f - t)\, \dot{\bar{s}}_1 + \bar{s}_1}{(t_f - t)^2} + \Phi sgn(\bar{s}_2) \right\} \quad [24]$$

where the coefficients for the second diagonal matrix $\Phi = diag[\Phi_1 \Phi_2 \Phi_3]$ can be selected such that,

$$\Phi_i = \frac{s_{2i_0}}{t_f^*} \quad [25]$$

where $t_f^* = n t_f, n < 1$. Recall that t_f is the prescribed time of flight, thus, the second sliding surface reaches zero in the finite time such that $t_f^* < t_f$. To demonstrate this property, substitute the acceleration command derived in Eq. [24] into the first time derivative of the second sliding surface vector in Eq. [21] to obtain,

$$\dot{\bar{s}}_2 = \Phi sgn(\bar{s}_2) \quad [26]$$

Further, noting that the vector $\bar{s}_2$ retains the same sign until reaching zero, the previous equation in Eq. [26] can be explicitly integrated,

$$\bar{s}_2(t) = s_{2i_0} \left(1 - \frac{t}{t_f^*} \right) \quad [27]$$

It is now apparent that the second sliding surface vector is driven to zero as $t \to t_f^*$. Finally, the derived control law is proven to be globally stable.

III.II MSSG under uncertainty

The acceleration command derived in Eq. [24] does not currently accommodate unmodeled perturbing effects. Now consider the augmented system with an unknown or unmodeled perturbing acceleration, $\bar{a}_P$,

$$\dot{\bar{\rho}} = \bar{v} \quad [28]$$

$$\dot{\bar{v}} = \frac{\partial U}{\partial \bar{\rho}} + \bar{a}_c + \bar{a}_p \quad [29]$$

The first derivative of the Lyapunov function V_2 becomes,

$$\dot{V}_2 = \bar{s}_2^T \dot{\bar{s}}_2 = \bar{s}_2^T \left[\bar{a}_P(t) - \Phi sgn(\bar{s}_2)\right] \quad [30]$$

Thus, to guarantee that $\dot{V}_2$ is negative definite, the gains Φ_i are selected such that $\Phi_i > max\left|a_{P_i}^{max}\right|$. The second Lyapunov function is decrescent and negative definite, thus, the Lyapunov stability theorem for non-autonomous systems guarantees that $\bar{s}_2 \rightarrow \bar{0}$ when $t \rightarrow t_f^*$, and consequently, $\bar{s}_1, \dot{\bar{s}}_1 \rightarrow \bar{0}$ when $t \rightarrow t_f$. Finally, provided that a upper bound for each component in the unmodeled perturbing acceleration is available, the MSSG control law is globally stable. The derived law supplies a robust control for the spacecraft in the vicinity of a pair of massive bodies.

III.III MSSG with Bounded Control

In the general formulation for the MSSG acceleration command, no explicit upper limit for the computed acceleration is enforced, that is, the control is unbounded. In practical applications, the feasible thrust magnitude may be limited; thus, a strategy to enforce bounded acceleration while preserving the direction of the computed acceleration is proposed. Consider the following control command, modified for boundedness,

$$\bar{a}_c = \begin{cases} \bar{a}_c & \text{if } \|\bar{a}_c\| < T_{MAX}, \\ T_{MAX}\frac{\bar{a}_c}{\|\bar{a}_c\|} & \text{if } \|\bar{a}_c\| \geq T_{MAX}. \end{cases} \quad [31]$$

where T_{MAX} is the maximum allowed acceleration command. Recall that current technology for low-thrust engines offers feasible thrust levels of approximately 100 mN. Assuming a spacecraft wet mass of 500 kg, the maximum thrust corresponds to a maximum acceleration of $T_{MAX} = 2 \times 10^{-4}$ m/s^2. This modified control input guarantees that the acceleration that is applied to guide the spacecraft remains within a feasible limit.

IV. DESIGN STRATEGY FOR PERIODIC ORBIT TRACKING WITH PRIMARY SHAPE UNCERTAINTY

The objective in this analysis is a strategy to maintain a spacecraft along a path that exhibits some desirable characteristics. Employing the multiple sliding surfaces guidance method, an acceleration command law is derived that delivers a spacecraft from an initial state to a desired state. Also, the guidance law is demonstrated to achieve global stability for the closed-loop system. In practical applications, such as mission scenarios that involve close proximity of a spacecraft within a binary system of asteroids, the exact physical properties of the massive bodies in the system are not known. It is reasonable to assume sufficient knowledge of the system to construct an 'estimated' model of the system that approximates the actual properties of the 'true' system.

IV.I Strategy

A strategy to maintain a spacecraft near a desirable path with limited knowledge concerning the primary system is introduced. First, a reference periodic orbit is computed for an estimated primary system model. Then, a scheme is constructed incorporating multiple sliding surfaces guidance to maintain the spacecraft near the reference. Within the context of mission scenarios that involve proximity to the primary system, it is not, in general, desirable to continuously operate the propulsive subsystem. For instance, during intervals of data collection such as science measurements, it may be important that the spacecraft is subject to minimal internal perturbations. Within this context, a 'coast and thrust strategy' is proposed. The spacecraft coasts until it reaches a prescribed deviation from the reference path, at which point the spacecraft is driven back to the reference path within a defined time. This process is repeated as necessary such that the spacecraft orbit is maintained.

IV.II Reference Trajectory

To explore the dynamical behavior of a third body in the vicinity of two irregular primaries, periodic orbits are of special interest. A differential corrections based technique is employed to compute a trajectory that is periodic in the nonlinear regime given some initial guess. Particular families of periodic orbits within this regime are labeled resonant orbits and the classical two-body problem is leveraged to generate an initial guess. Within the context of a restricted two-body problem, consider two bodies, A and B, that orbit a primary body. The primary body is massive while bodies A and B are assumed massless, consistent with the restricted two-body problem model. Body B is defined to be in resonance with body A if it completes p orbits with respect to the primary in the same time that body A achieves exactly q orbits.[22] In this definition, p and q are two positive integers where p is associated with body B and q refers to the period of body A. For instance, a spacecraft in a $1:2$ resonance with the Moon completes one revolution around Earth in the same time that the Moon completes two periods.

Using this restricted two-body problem to produce an initial guess for a resonant orbit given some resonant ratio $p:q$, an orbit that is periodic and possesses, approximately, the two-body resonant ratio is computed in the three-body regime. Employing a continuation method in a higher-fidelity model, a family of resonant orbits, or, a set of orbits that share some common characteristics, is computed. Also, exploiting bifurcations within the planar resonant family, other families with the same resonance ratio that include symmetric or asymmetric three-dimensional trajectories can be generated.

IV.III MSSG with Perturbing Acceleration

Consider two models for the binary system. First, a 'true' model is one that corresponds to the actual in situ system; the true gravitational model is, in fact, unknown or at least uncertain, prior to the mission. The true system is represented by the higher-fidelity dynamical model, that is, each primary is modeled as a polyhedron. Then, an 'estimated' system, that is, an approximate system, is constructed based upon prior knowledge of the system and is employed for trajectory design. The motion of the spacecraft is numerically integrated with the EOM and the gravity model that correspond to the higher-fidelity polyhedron model while the acceleration command is computed solely based upon the lower-fidelity estimated system, that is, assuming the system is comprised of ellipsoidal massive bodies. The deviation between the total gravitational acceleration exerted by the true and the estimated system is defined as the perturbation acceleration vector $\bar{a}_p$ in Eq. [28]. The control law is globally stable if the second matrix gains Φ are selected such that,

$$\dot{V}_2 = \bar{s}_2^T \left[\bar{a}_P(t) - \Phi sgn(\bar{s}_2)\right] < 0 \qquad [32]$$

that is, such that $\Phi_i > max\left|a_{P_i}^{max}\right|$.

IV.IV Validation with Fictitious Binary Model

The proposed strategy is initially validated exploiting a fictitious primary system model. For a given reference trajectory, the 'coast and thrust' scheme is simulated.

Primary system models

Consider a fictitious primary system such that the primary P_1 is a scaled model of the asteroid Eros and the second primary is a spheroid. For the true system, each primary, P_1 and P_2, is constructed as a constant density polyhedron. Also, the motion of the primary system is assumed to be consistent with a synchronous system, that is, each primary appears fixed as viewed in the rotating frame. The estimated system is then an ellipsoid-sphere model with an elongated primary such that the largest equatorial P_1 radius equals 5 km, the ellipsoid axes ratios are $\beta = \gamma = 0.5$, the primary mass ratio is $\nu = 0.2$, and the primary distance is $r = 6$.

Reference trajectory

The reference trajectory for this application is a sample three-dimensional $1:2$ symmetric resonant orbit as computed with the estimated system, and illustrated in Figure 2.

Simulation

For the fictitious primary system model and the sample reference trajectory, the 'coast and thrust' scheme is simulated. The initial state to generate the reference orbit from the ellipsoid-sphere system is numerically integrated using the EOM with the gravitational acceleration computed using the polyhedron model until the spacecraft state reaches a predetermined deviation from the reference path. Then, using the final state along the coast arc as the new initial condition state vector for the controlled trajectory, the EOM incorporating the MSSG acceleration command, as computed with the ellipsoid-sphere model, is numerically integrated for the prescribed finite time t_f. For this simulation, the time of flight is selected as $t_f = 1/5P$ where P is the period of the reference orbit, $t_f^* = 1/2t_f$, i.e., $n = 1/2$, the gain matrix Λ is $\Lambda = [5\,5\,5]$, and the matrix Φ is selected such that $\Phi_i > max\left|a_P i^{max}\right|$. In Figure 3 are illustrated the reference trajectory, the uncontrolled trajectory using the reference orbit initial state, the coast arcs, and the controlled arcs in black, red, blue, and purple, respectively. Visually, the design objective is achieved for the two thrust arcs that are apparently required to maintain the spacecraft in orbit for one revolution along the reference trajectory. Further, the acceleration profile and the sliding surface vector time histories are illustrated in Figure 4. The second and first sliding surfaces converge to zero at t_f^* and t_f for the two controlled arcs, respectively. Note that, although not yet incorporated as a constraint, the magnitude of the acceleration command remains smaller than the reference maximum value of 2×10^{-4} m/s^2. Also, as expected, the tracking errors also converge to zero, as depicted for the first arc in Figure 5. Finally, this example successfully demonstrates the proposed 'coast and thrust' strategy. The acceleration command computed with the MSSG algorithm allows the spacecraft to successfully reach the reference path. To maintain the spacecraft in orbit for one revolution along the desired trajectory, two coast arcs and two controlled arcs are sufficient.

IV.V MSSG with Bounded Control Input

As demonstrated in the previous example, the proposed scheme successfully drives the spacecraft state to the reference path under the perturbing accelerations

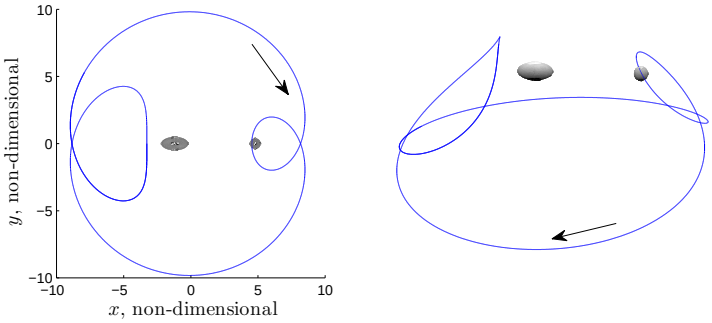

Fig. 2: Reference trajectory: resonant 1:2 3D symmetric orbit in the EE3BP

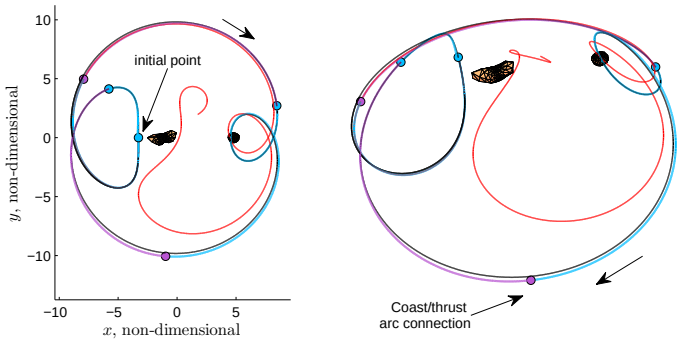

Fig. 3: Simulation under uncertainty. Uncontrolled (red), coast (blue), and thrust (purple) arcs.

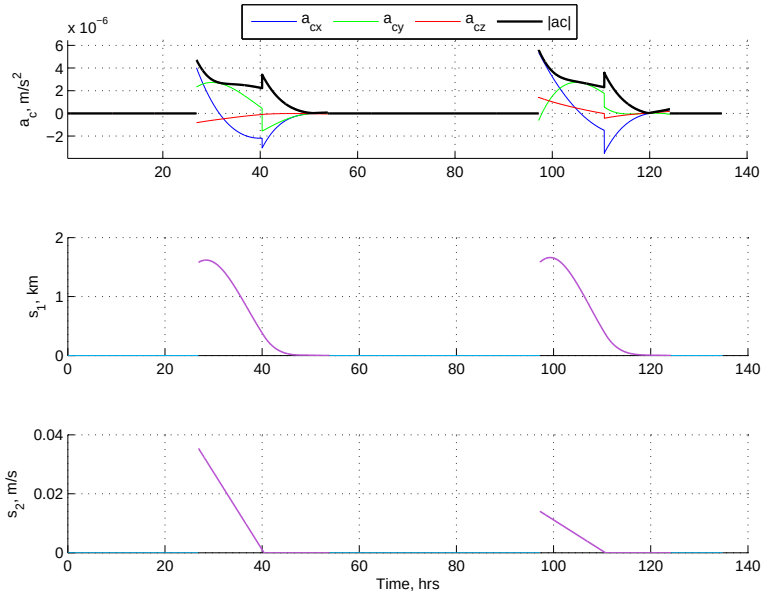

Fig. 4: Acceleration and sliding surfaces history

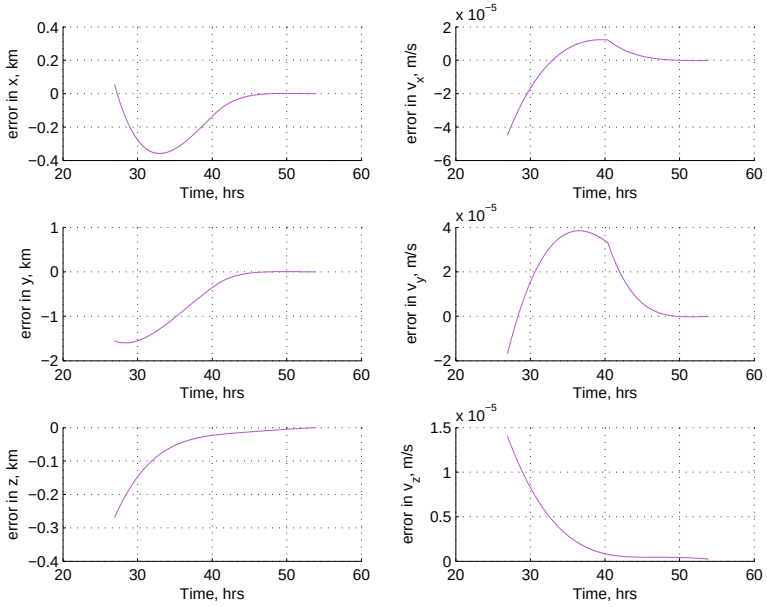

Fig. 5: Error history: thrust arc 1

that are due to uncertainties in the system physical properties. The acceleration command magnitude is reasonable with respect to the currently available technology for the specific simulation in Section IV.IV. However, no explicit upper limit for the computed acceleration is enforced, that is, the control is unbounded. To assess the validity of the bounded control strategy, as introduced in Section III.III, the same simulation is repeated. Additionally, a velocity perturbation is applied to the initial state on the reference path to exaggerate the drift rate from the reference trajectory during the first phase of the simulation, that is, when the spacecraft is nominally coasting under the natural dynamics. Also, the predefined deviation from the reference solution that triggers a thrust arc is significantly increased. Such a scenario may be analogous to a spacecraft experiencing a failure and drifting from the reference solution beyond the prescribed boundary limits. Assuming the spacecraft eventually recovers, the objective of this simulation is to assess the capability of the proposed scheme to recover the reference orbit, under a bounded control input, from an initially large deviation. Consider a first test case with an initial velocity perturbation in nondimensional units equal to $\delta\bar{v} = \begin{bmatrix} 0 & -5\times10^{-2} & 0 \end{bmatrix}$, and initially assume that the MSSG controller employs an unbounded control input. The resulting coast arc and the controlled arc are illustrated in Figure 6(a) along with the reference trajectory in blue, purple, and black, respectively. As designed, at the end of the initial coast arc, the spacecraft is located further from the reference compared to the previous simulation. Then, the MSSG control law successfully drives the spacecraft back to the reference path; however, the acceleration command magnitude exceeds the maximum allowed acceleration T_{MAX}. Now consider the same problem with a bounded acceleration command. The trajectory arcs that result from the simulation are illustrated in Figure 6(b). Again, the MSSG control law successfully drives the spacecraft back to the reference orbit and the controlled arc, with bounded acceleration, closely resembles the unbounded controlled path. However, as illustrated in Figure 7, the acceleration command does not exceed the maximum allowable acceleration yet still achieves the design objective, as depicted by the two sliding surface vectors converging to zero within the allocated finite time. For this first simulation, the bounded MSSG successfully drives the spacecraft from a distant state relative to the desired path back to the reference solution while the acceleration command is bounded to remain within a feasible maximum value.

To further assess the performance of the bounded controller, additional test cases are examined with a variety of initial velocity perturbations. Consider the scenarios with initial velocity perturbations, $\delta\bar{v}_1 = \begin{bmatrix} -1\times10^{-2} & -1\times10^{-2} & 0 \end{bmatrix}$, $\delta\bar{v}_2 = \begin{bmatrix} 0 & -5\times10^{-2} & 0 \end{bmatrix}$, and $\delta\bar{v}_3 = \begin{bmatrix} 0 & -3\times10^{-2} & -2\times10^{-2} \end{bmatrix}$. The results from the three scenarios are represented in Figures 8 and 9. First, the controlled arcs for cases 1 through 3 are illustrated in purple, green, and orange, respectively, in Figure 8. Visually, the design objective is achieved in all three cases. Next, the sliding surface vectors converge to zero as expected for the three scenarios as depicted in Figure 9. Also represented in this figure is the magnitude of the acceleration command and, for the three cases, the control input is again bounded by the upper value T_{MAX}. In summary, the robust MSSG controller is augmented with a bounded control input. To assess the performance of the bounded control, a fictitious scenario is introduced where the spacecraft is initially far from the reference.

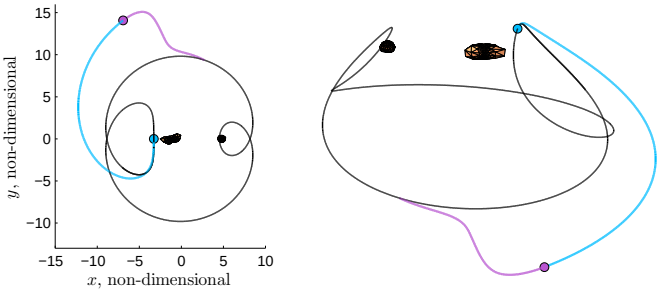

a) Unbounded input

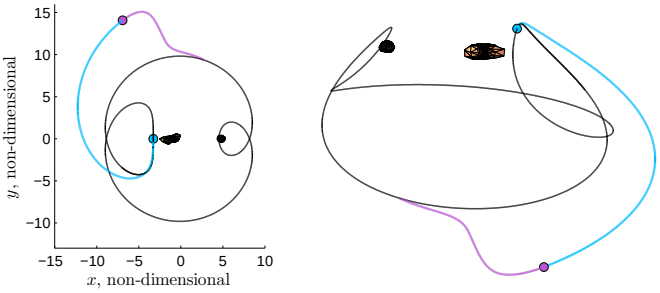

b) Bounded input

Fig. 6: Simulation under uncertainty: coast (blue) and thrust (purple) arcs

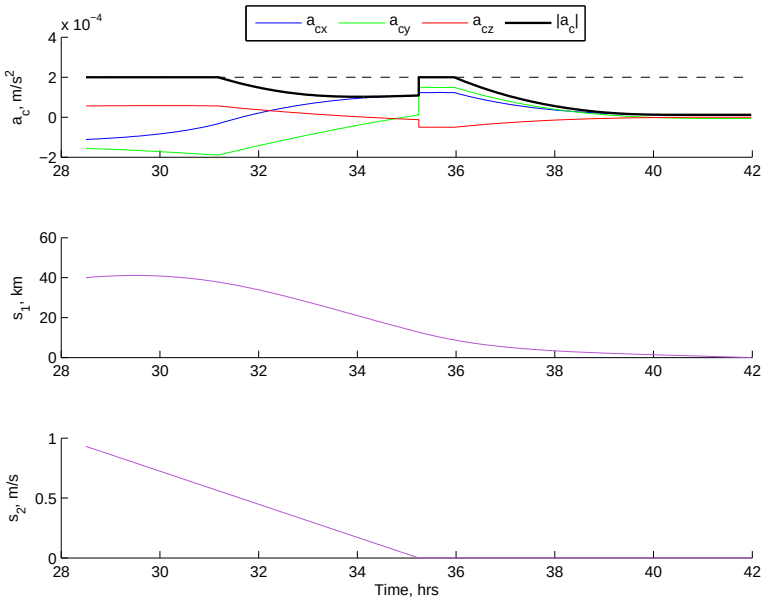

Fig. 7: Acceleration and sliding surfaces history for bounded input simulation

The guidance strategy is active as the motion evolves. Without bounds on the control input, the MSSG successfully drives the spacecraft back to the reference but the acceleration command magnitude exceeds the current technology that is assumed to be available for low thrust engines. A strategy for bounded control that preserves the direction of the computed acceleration vector is demonstrated.

V. APPLICATION TO KNOWN BINARY 1999 KW4

A design strategy to maintain a spacecraft near a reference path with some desirable characteristics is proposed assuming limited a priori knowledge of the primary system. The scheme is initially validated with a fictitious binary system model and a next step in the investigation is an extension to a known binary system.

V.I Primary System Model: 1999 KW4

Consider the well-known Near Earth Asteroid (NEA) 1999 KW4. The first step in the analysis is the construction of both true and estimated models for the motion of the given primary system.

Primary shape model

For 1999 KW4, a medium resolution polyhedron shape model is illustrated in Figure 10 for the primary and secondary component that comprise the KW4 binary asteroid. This shape model is derived from the full resolution model constructed in Ostro et al.[23] Also, some representative physical parameters for each body are summarized in Table 1. The primary exhibits the characteristic 'walnut' shape while the secondary, much smaller in size, is a very oblate and significantly elongated body.

Table 1: 1999 KW4 shape model

	A_X (km)	A_Y (km)	A_Z (km)
Primary	1.53	1.49	1.35
Secondary	0.57	0.46	0.35

density (kg m^{-3})	rotation period (hr)
1970	2.76
2810	17.42

Primary motion simulation

The irregular shape of each of the two bodies directly affects the relative motion of the two primaries; the fully coupled motion of the two-body system is modeled and numerically integrated, as outlined in Section II.II. The initial orbital conditions and configuration for such a simulation are summarized in Table 2 for the primary orbital motion, in terms of semi-major axis and eccentricity, and the initial orientation of both bodies. The angles ψ_i, θ_i, and ϕ_i correspond to the Euler angles for a $3-1-3$ sequence and $i = 1, 2$ for the primary and secondary, respectively. The mutual motion, both orbital and rotational, is numerically integrated for approximately 15 revolutions of the primary system. Recall that the computation of the mutual force, as well as the torque that one body exerts on the other, at each time step during the numerical integration process relies on an infinite series expansion of the gravitational potential. In this simulation, only the first five terms in this series are retained, that is, four orders beyond the point mass solution. Selected results from this simulation appear in Figure 11. As expected, the irregular shape of the body directly impacts the mutual orbital motion, as clearly illustrated by the oscillating semi-major axis and eccentricity as time evolves; also, it is directly apparent in the primary-centered inertial view of the trajectory. Although not presented here, the attitude of each body is also influenced by the mutually irregular shapes. For this problem, energy and angular momentum are conserved, however, it is sometimes challenging to achieve conservation of these quantities, to some specified tolerance, during the numerical integration process over long time intervals. In this analysis, the symplectic algorithm allows energy and angular moment to be conserved within reasonable and bounded values throughout the simulation.

Table 2: 1999 KW4 initial conditions

a (km)	e	ψ_1 (deg)	θ_1 (deg)
2.54	0.01	27.04	10

ϕ_1 (deg)	ψ_2 (deg)	θ_2 (deg)	ϕ_2 (deg)
-83.93	0	0	180

V.II Reference Trajectory

The reference trajectory is a three-dimensional symmetric $1:2$ resonant orbit computed for a sample synchronous ellipsoid-ellipsoid system consistent with the dimensions of the 1999 KW4 primary bodies, as illustrated in Figure 12. In Table 3 are summarized the characteristics that are associated with the 1999 KW4 model, including the system mass ratio, μ, the primary distance separation, r, and the ellipsoid axes ratios, α_i, β_i, γ_i for the primary P_i.

Table 3: Characteristic quantities associated with the 1999 KW4 model

μ	r	β_1	γ_1	β_2	γ_2
0.0541	3.64	1	0.845	0.8109	0.6112

V.III Simulation

The proposed guidance strategy is now applied to the known binary system 1999 KW4. In addition to the

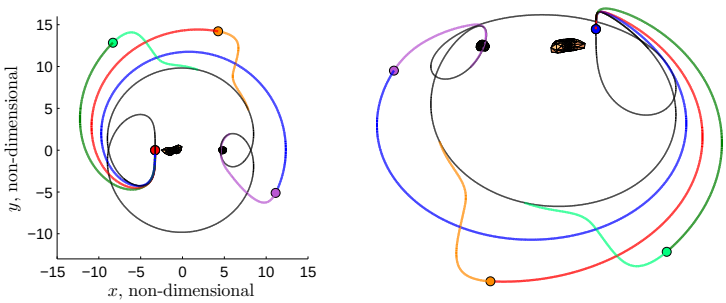

Fig. 8: Additional simulations under uncertainty with bounded input

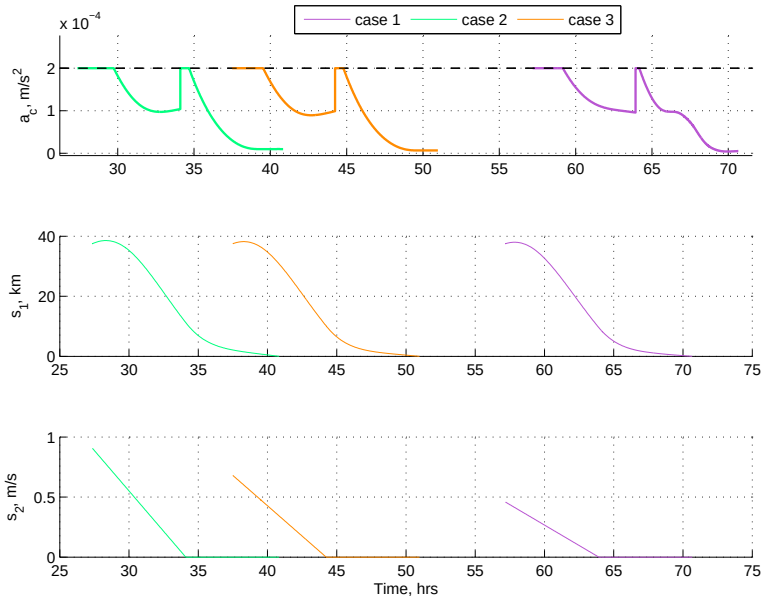

Fig. 9: Acceleration and sliding surfaces history for bounded input simulations

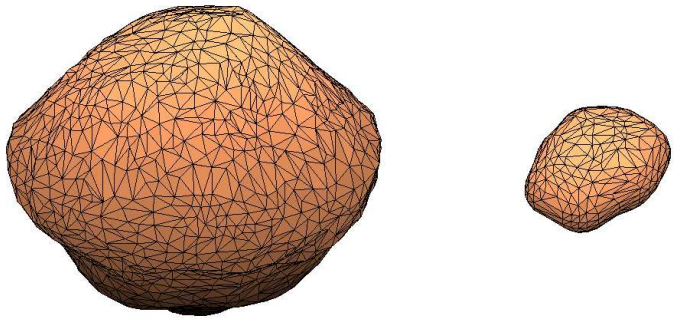

Fig. 10: 1999 KW4 shape model: primary (left) and secondary (right)

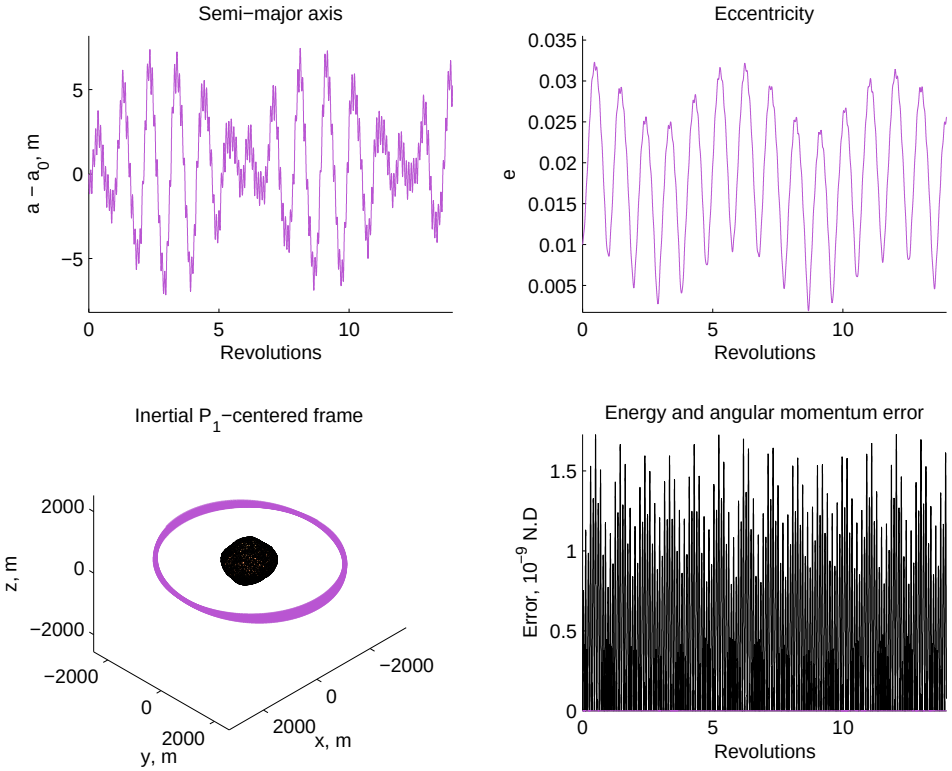

Fig. 11: 1999 KW4 simulation

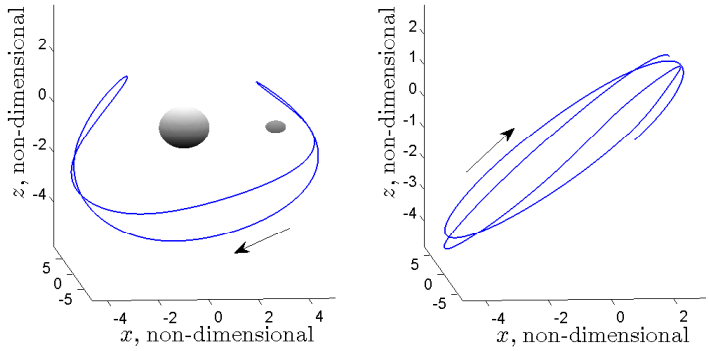

Fig. 12: Reference trajectory: resonant 1:2 3D symmetric orbit in the EE3BP

perturbing acceleration due to the uncertainty in the physical and dynamical properties of the primary system, solar radiation pressure exerted on the spacecraft is also incorporated into the simulation. Note that the magnitude of both perturbing accelerations remain smaller than the reference maximum value T_{MAX}. The results of the simulation incorporating the MSSG guidance law appears in Figure 13, where the reference trajectory, the coast arcs, and the controlled arcs are plotted in red, blue, and purple, respectively. In this simulation, the allowed deviation from the reference path is arbitrarily selected to equal 1.25 nondimensional distance units, the time of flight is specified as $t_f = 1/10P$, $n = 1/3$, that is, the second sliding surface vector reaches zero at $t_f^* = t_f/3$. The time constants are also arbitrary. For test values of t_f^* equal to values between $1/4$ and $3/4$, similar simulations result in the same successful outcome. A relatively small t_f value allows short thrust arcs to maximize scientific activities while requiring a larger control effort. In contrast, a longer time of flight would allow a smaller thrust magnitude, if required. The number of coast and thrust arcs is then determined autonomously; the design objective is achieved for the two thrust arcs

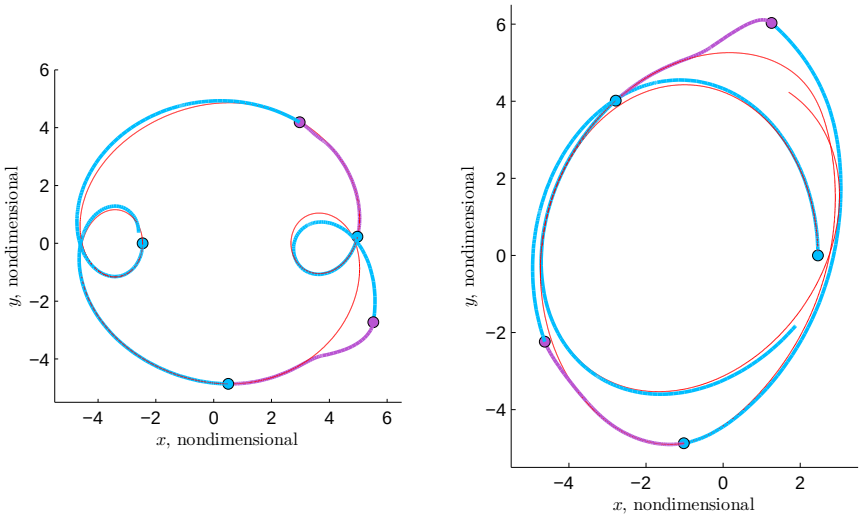

Fig. 13: Simulation under uncertainty with bounded input for 1999 KW4 viewed in rotating (left) and inertial (right) frame. Reference (red), coast (blue) and thrust (purple) arcs

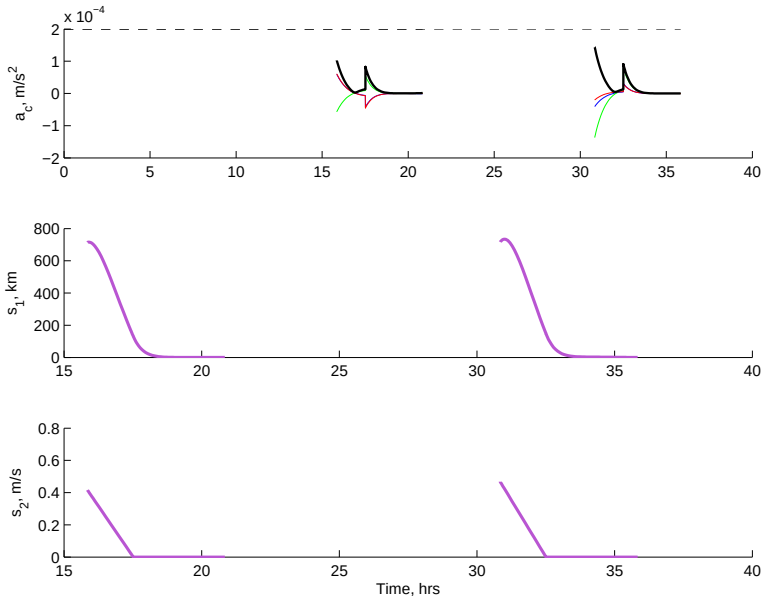

Fig. 14: Acceleration and sliding surfaces history

that are required to maintain the spacecraft in orbit for one revolution along the reference trajectory. The acceleration profile and sliding surface vector time histories are illustrated in Figure 14. The first and second sliding surfaces converge to zero at t_f and t_f^* for the two controlled arcs, respectively. Note that the magnitude of the acceleration command remains smaller than the reference maximum value of 2×10^{-4} m/s^2. Finally, this application successfully demonstrates the proposed 'coast and thrust' strategy for an actual binary system. The scheme is robust against unmodeled accelerations due to uncertainties in the physical and dynamical properties of the primary system, as well as the solar radiation pressure.

VI. CONCLUSION AND FUTURE WORK

The multiple sliding surfaces guidance algorithm is employed to derive an acceleration command for the control of a spacecraft in the vicinity of a pair of irregular bodies. The control law is demonstrated to achieve the design objective, that is, tracking a desired solution, in a finite time. Most importantly, the control law is globally stable. The guidance law is also robust and globally stable against unmodeled accelerations, provided an upper bound for the perturbing acceleration is available. A trajectory design strategy to maintain a spacecraft near reference third-body trajectories that exhibit some desired characteristics is constructed. In practical applications, the exact physical properties of the massive bodies in the system are not known. It is reasonable to assume sufficient knowledge to construct

an 'estimated' model that approximates the properties of the 'true' system. For the true system, each primary is modeled as a polyhedron and the 'estimated' system is an ellipsoid-ellipsoid model. Then, to maintain the spacecraft in orbit near a desired reference trajectory, a 'coast and thrust' scheme is proposed. The spacecraft coasts until it reaches a prescribed deviation from the reference path, at which point the spacecraft is driven back to the reference within a defined time. This process is automated to allow successive coast and thrust arcs to maintain the spacecraft orbit. Based upon the simulations, the design strategy achieves the objective under the perturbing acceleration due to the uncertainty in the system physical properties. The acceleration command magnitude is, in general, reasonable with respect to the assumed current available technology. Nevertheless, the robust MSSG controller is augmented with a bounded control input that preserves the direction of the computed acceleration vector to better represent an actual mission scenario. Also, a simulation that includes the solar radiation pressure on the spacecraft as an additional perturbation near a known binary system, 1999 KW4, is introduced. In this analysis, the acceleration command is computed in terms of Cartesian components as expressed in the inertial frame. Future work includes the incorporation of additional constraints to better capture realistic thrust conditions based upon the attitude of the spacecraft. Also, currently, the acceleration command can be arbitrarily small while, in practical applications, in addition to a maximum deliverable thrust, engines also are constrained by a minimum feasible thrust. Bounded control for the lower limit can also be explored.

VII. ACKNOWLEDGEMENTS

The authors are grateful for access to the Rune and Barbara Eliasen Visualization Laboratory at Purdue University in support of this research.

REFERENCES

[1]R. W. Farquhar, D. W. Dunham, and J. V. McAdams, "NEAR Mission Overview and Trajectory Design, Special Issue on the Near Earth Asteroid Rendezvous Mission," *J. Astronautical Sciences*, vol. 43, no. 4, pp. 353–371, 1995.

[2]M. D. Rayman, T. C. Fraschetti, C. A. Raymond, and C. T. Russell, "Dawn: A mission in development for exploration of main belt asteroids Vesta and Ceres," *Acta Astronautica*, vol. 58, pp. 605–616, June 2006.

[3]M. Y. Marov, V. S. Avduevsky, E. L. Akim, T. M. Eneev, R. S. Kremnev, S. D. Kulikov, K. M. Pichkhadze, G. A. Popov, and G. N. Rogovsky, "Phobos-Grunt: Russian sample return mission," *Advances in Space Research*, vol. 33, pp. 2276–2280, Jan. 2004.

[4]K.-H. Glassmeier, H. Boehnhardt, D. Koschny, E. Khrt, and I. Richter, "The rosetta mission: Flying towards the origin of the solar system," *Space Science Reviews*, vol. 128, no. 1-4, pp. 1–21, 2007.

[5]http://osiris-rex.lpl.arizona.edu/. Last accessed 02-23-2013.

[6]J. L. Margot, M.C. Nolan, L.A.M. Benner, S.J. Ostro, R.F. Jurgens, J.D. Giorgini, M.A. Slade, and D.B. Campbell, "Binary asteroids in the near-earth object population," *Science*, vol. 296, pp. 1445–1448, 2002.

[7]J. Bellerose and D. J. Scheeres, "Periodic orbits in the vicinity of the equilateral points of the restricted full three-body problem," in *AAS/AIAA Astrodynamics Specialist Conference*, August 7-11 2005.

[8]L. Chappaz and K. Howell, "Trajectory Exploration within Binary Systems Comprised of Small Irregular Bodies," in *23rd AAS/AIAA Space Flight Mechanics Meeting*, (Kauai, Hawaii), February 2013.

[9]E. G. Fahnestock and D. J. Scheeres, "Simulation and analysis of the dynamics of binary near-Earth Asteroid (66391) 1999 KW4," *Icarus*, vol. 194, pp. 410–435, 2008.

[10]E. G. Fahnestock and D. J. Scheeres, "Characterization of Spacecraft and Debris Trajectory Stability within Binary Asteroid Systems," in *AIAA/AAS Astrodynamics Specialist Conference and Exhibit*, (Honolulu, Hawaii), August 18-21, 2000.

[11]L. Chappaz, "The Dynamical Environment in the Vicinity of Small Irregularly-Shaped Bodies and Application to Asteroids." M.S. Thesis, School of Aeronautics and Astronautics, Purdue University, West Lafayette, Indiana, December 2011.

[12]L. Chappaz and K. Howell, "Bounded Orbits near Binary Systems Comprised of Small Irregular Bodies," in *AIAA/AAS Astrodynamics Specialist Conference*, (San Diego, California), August 2014.

[13]R. Furfaro, D. O. Cersosimo, and D. R. Wibben, "Asteroid Precision Landing Via Multiple Sliding Surfaces Guidance Techniques," in *AAS/AIAA Astrodynamics Specialist Conference*, (Girdwood, Alaska), July 2011.

[14]R. Furfaro, D. Cersosimo, and J. Bellerose, "Close Proximity Asteroid Operations Using Sliding Control Modes," in *22nd AAS/AIAA Space Flight Mechanics Meeting*, (Charleston, South Carolina), January 2012.

[15]D. Scheeres, "Stability of the planar full 2-body problem," *Celestial Mechanics and Dynamical Astronomy*, vol. 104, no. 1-2, pp. 103–128, 2009.

[16]T. Lee, M. Leok, and N. H. McClamroch., "Lie Group Variational Integrators for the Full Body Problem in Orbital Mechanics," *Celestial Mechanics and Dynamical Astronomy*, vol. 98, no. 2, pp. 121–144, 2007.

[17]E. Fahnestock and D. Scheeres, "Simulation of the full two rigid body problem using polyhedral mutual potential and potential derivatives approach," *Celestial Mechanics and Dynamical Astronomy*, vol. 96, no. 3-4, pp. 317–339, 2006.

[18]M. Hirabayashi and D. Scheeres, "Recursive computation of mutual potential between two polyhedra," *Celestial Mechanics and Dynamical Astronomy*, vol. 117, no. 3, pp. 245–262, 2013.

[19]R. A. Werner, "The Gravitational Potential of a Homogeneous Polyhedron or Don't Cut Corners," *Celestial Mechanics and Dynamical Astronomy*, vol. 59, no. 3, pp. 253–258, 1993.

[20]A. Levant, "Sliding Order and Sliding Accuracy in Sliding Mode Control," *International Journal of Control*, vol. 58, no. 6, pp. 1247–1263, 1993.

[21]A. Levant, "Higher-order sliding modes, differentiation and outputfeedback control," *International Journal of Control*, vol. 76, pp. 924–941, 2003.

[22]M. Vaquero, *Spacecraft Transfer Trajectory Design Exploiting Resonant Orbits in Multi-Body Environments*. PhD Dissertation, School of Aeronautics and Astronautics, Purdue University, West Lafayette, Indiana, August 2013.

[23]S. J. Ostro, J.-L. Margot, L. A. M. Benner, J. D. Giorgini, D. J. Scheeres, E. G. Fahnestock, S. B. Broschart, J. Bellerose, M. C. Nolan, C. Magri, P. Pravec, P. Scheirich, R. Rose, R. F. Jurgens, E. M. De Jong, and S. Suzuki, "Radar imaging of binary near-earth asteroid (66391) 1999 kw4," *Science*, vol. 314, no. 5803, pp. 1276–1280, 2006.